Proceedings of The Institute of Acoustics

FLUCTUATIONS IN ACOUSTIC TRANSMISSION LOSS: COMPARISONS BETWEEN MEASURED DATA AND PREDICTIONS OF THE SAFARI/PARABOLIC EQUATION NUMERICAL MODELS

Hassan B. Ali (1), Joseph V. Soileau (1), Reuben P. Wooten (2), and Gerard J. Tango (1)

(1) Naval Ocean Research and Development Activity, Ocean Acoustics and Technology Directorate, NSTL, MS 39529-5004, USA
(2) ODSI Defense Systems, Inc., 6110 Executive Blvd., Rockville, MD 20852, USA

ABSTRACT

The results of acoustic transmission loss measurements in a shallow-water area of the North Atlantic have revealed significant fluctuations in the acoustic intensity levels received by a 60-km distant vertical array of hydrophones. The attempt to attribute these fluctuations to easily identifiable properties of the medium is frustrated by the complexity of the latter. An added complication arises from the location of the measurement site in a geographical area characterized by the convergence of two major water masses of differing environmental properties, viz., Arctic water and Atlantic water. Moreover, the resulting Polar oceanic front is not stationary but, rather, oscillates with semidiurnal tidal periodicity.

Propagation factors tentatively identified as contributors to the acoustic fluctuation include the steep gradients in environmental parameters arising from the different water masses, changes in water depth, currents, and possibly other effects. Numerical studies were performed in an attempt to determine the general trends expected of the propagation in this environment. In particular, using simplified models of the test environment, computations were made with SAFARI FFP and a wide-angle version of the Parabolic Equation model (IFDPE). Although neither model by itself is entirely adequate for the environment considered, both range-dependence and ocean-bottom shear being of interest, the combination does provide some insight into the suspected phenomena.

I. INTRODUCTION

The propagation of sound in the ocean is inevitably accompanied by fluctuations in the amplitude and phase of an acoustic signal received at large distances from the source. The fluctuations manifest not only changing patterns of interaction with the bottom and surface, particularly important in shallow water propagation, but also passages of the wave through time-varying inhomogeneities in the ocean medium. The resulting fluctuations, or scintillations, in acoustic intensity are analogous to the twinkling of stars arising from multiple scattering of lightwaves in the irregular layers of the upper atmosphere. The variability in acoustic propagation can be considered to arise from variations in the index of refraction, or sound velocity, of the medium, which, in turn, are induced by a variety of ocean processes covering a wide range of temporal and spatial scales [1]. This paper will compare the results of acoustic transmission loss measurements exhibiting environmentally induced fluctuations with predictions based on standard numerical models.

II. THEORETICAL (DETERMINISTIC) APPROACHES

The detailed explanation of the measured results would, perforce, have to consider both random and deterministic aspects of the propagation. The objective here is far less ambitious than the preceding goal which, in any case, is most

FLUCTUATIONS IN ACOUSTIC TRANSMISSION LOSS: COMPARISONS BETWEEN MEASURED DATA AND PREDICTIONS OF THE SAFARI/PARABOLIC EQUATION NUMERICAL MODELS

likely unattainable at present. Both the complexity of the propagation environment and the inherent limitations of current numerical models preclude this possibility. Here, attention is confined to the investigation of the general trends expected of the data, using two well-established numerical models and assuming only deterministic propagation behavior.

The models used are SAFARI, the newest version of the Fast Field Program (FFP), from SACLANTCEN [2], and IFDPE, a wide-angle version of the Parabolic Equation (PE) method from NORDA/NUSC [3].

1. Description of Numerical Models Used

The mathematical details of SAFARI and IFDPE are given elsewhere. A brief description is appropriate here, however, since it will facilitate the interpretation of the results.

The basis of the models is, of course, the wave equation for a harmonic point source:

$$\nabla^2\phi(x,y,z) + [\omega/c(x,y,z)]^2\phi(x,y,z) = -\delta(x - x_o)\delta(y - y_o)\delta(z - z_o) \qquad (1)$$

where $\phi(x,y,z)$ is the velocity potential, $c(x,y,z)$ is the sound speed in the medium, ω is the angular frequency, and the source is located at the point (x_o,y_o,z_o), z being the depth coordinate.

a. SAFARI

The SAFARI model (SACLANTCEN Fast Field Program for Range-Independent Environments), like the earlier versions of the FFP due to Dinapoli and Kutschale, solves equation (1) for a "horizontally stratified ocean." In this case, the sound-speed is a function only of depth, that is, $c(x,y,z)$ is just $c(z)$; further the bottom is flat. For such a range-independent environment, a useful solution of (1) is the Fourier decomposition of the acoustic field into an infinite set of horizontal waves:

$$\phi(x,y,z) = \frac{1}{2\pi}\int_0^\infty G(\vec{\eta},z)e^{-i\vec{\eta}\cdot\vec{r}}\,d^2\vec{\eta} \qquad (2)$$

where $G(\vec{\eta},z)$ is the depth-dependent Green's function, and η is the horizontal wavenumber of the individual plane waves. Exploiting the axial symmetry of the wave field, one can use polar coordinates to replace the two-dimensional Fourier transform by a Fourier-Bessel (Hankel) transform:

$$\phi(r,z) = \tfrac{1}{2}\int_{-\infty}^{\infty}\eta G(\eta,z)H_o^{(1)}(\eta,r)\,d\eta \qquad (3)$$

where $H_o^{(1)}(\eta,r)$ is the zeroth order Hankel function of the first kind. The asymptotic form of the Hankel function (valid for ranges greater than a few wavelengths from the source) can be used to transform (3) into the following convenient form:

FLUCTUATIONS IN ACOUSTIC TRANSMISSION LOSS: COMPARISONS BETWEEN MEASURED DATA AND PREDICTIONS OF THE SAFARI/PARABOLIC EQUATION NUMERICAL MODELS

$$\phi(r,z) = \frac{e^{-i\pi/4}}{2\pi r^{\frac{1}{2}}} \int_{-\infty}^{\infty} \eta G(\eta,z) e^{i\eta r} d\eta \qquad (4)$$

The $r^{-1/2}$ weighting factor indicates cylindrical spreading. Equation (4) is the starting point for numerical integration to obtain the acoustic field at a range r and depth z. This requires first that G (η,z) be solved (using (1) and (2)) for several values of η. The integration in (4) can then be performed rapidly using a Fast Fourier Transform (FFT) algorithm, resulting in the complex pressure ($p = -i\omega\rho\phi$) as a function of range. This entire procedure constitutes the FFP approach. The FFP technique provides the "full" solution to sound propagation in a multilayered liquid/solid environment since the complete spectrum is integrated. Thus, the solution is valid at long or short ranges (far- or near-field) and for discrete (normal) and continous (virtual, leaky) modes and evanescent (interface) waves. Understanding the behavior of the Green's function is essential to clarifying the differences between discrete, continuous, and evanescent modes in a particular environment. The Green's function or, more precisely, the FFP integrand, represents the propagating energy as a function of horizontal wavenumber. The singularities in the integrand (poles) represent discrete modes of propagation, the finite width of the responses indicating the presence of losses in the system. The demarcation between discrete and continuous modes is based on the critical angle, $\theta_c = \cos^{-1}(c_w/c_b)$ of the bottom, which depends on the compressional phase velocities in the water column c_w, and in the bottom, c_b. For grazing angles (measured with respect to the horizontal) less than θ_c much of the incident energy (all, if the bottom is lossless) is reflected, resulting in the propagation of discrete modes. For grazing angles greater than the critical angle, significant transmission into the bottom occurs, giving rise to continuous modes which, because they decay much more rapidly than $r^{-1/2}$, are largely confined to the near wave field. The interface, or boundary wave, travels at a phase velocity less than either the sound speed in water or the shear speed in the bottom. Its amplitude decays exponentially in a direction perpendicular to the interface (water/bottom in this case), its penetration depth being roughly one wavelength.

b. IFDPE

The Parabolic Equation (PE) method is a simplification of the wave equation for scattering that is mostly in the forward direction (paraxial approximation). Thus, the standard PE is intrinsically a narrow angle approximation, valid to about $\pm$20° about the horizontal. The numerical solution of the original PE employed the so-called "split step" FFT marching algorithm. The Implicit Finite-Difference PE (IFDPE), developed jointly by the Naval Ocean Research and Development Activity (NORDA) and the Naval Underwater Systems Center (NUSC) [3], uses a finite-difference solution technique and extends the angle coverage to about $\pm$40°. The advantage of the PE is that it can handle a range-dependent environment. Among its disadvantages are its inability to handle bottom-shear in a straightforward way and its omission of backscattering. Space limitations preclude further discussion of the PE.

FLUCTUATIONS IN ACOUSTIC TRANSMISSION LOSS: COMPARISONS BETWEEN MEASURED DATA AND PREDICTIONS OF THE SAFARI/PARABOLIC EQUATION NUMERICAL MODELS

III. EXPERIMENTAL RESULTS

1. Test Procedure

The experimental configuration for the North Atlantic test, conducted by SACLANTCEN, is shown in Figure 1. The two tracks, A-B and D-C represent the propagation paths for measurements conducted one year apart. For the configuration shown, broadband sources (explosives) were dropped at hourly intervals. The receivers were vertical arrays of hydrophones. Simultaneous samplings of the pertinent oceanographic parameters (sound speed, temperature, salinity, and density) were taken at both the source and receiver locations.

2. Characteristics of the Test Site

The North Atlantic test site is a very complex geological, oceanographic, and biological province and has been the object of many investigations [4]. The test site is located in an area affected by a large-scale permanent front resulting from the convergence of two water masses. In particular, at this location, cold, less saline Arctic water meets warmer Atlantic water to form the Polar oceanic front. The substantial differences in salinity and temperature of the two water-types (35 ppt and 6-7°C for the Atlantic vs. 34.6 ppt and about 0°C for the Arctic) cause the Polar front to be characterized by steep gradients in these parameters, with significant implications for sound propagation. An added complication arises from the changing position of the front, which oscillates with semidiurnal tidal periodicity.

The environmental conditions along the two paths shown in the figure were somewhat different. Although both tracks A-B and D-C cross the Polar front, in water changing from deep to shallow, track A-B is over a generally hard bottom (sand), while track D-C is over a generally soft bottom (sand, silt, clay). From the temporal variability point of view, however, a more fundamental difference between the two receiver locations arises from their relative proximity to the Polar front. In particular, station C is directly affected by movements of the front, the water above 20 m changing from Polar to Atlantic with an approximately 12h periodicity, while the waters below 20 m remain of the Polar type. In comparison, station B remains in virtually isothermal Polar water, north of the front, as shown schematically in Fig 1.

In effect, the Polar front serves as a demarcation line between two different propagation areas. To the north of the front, in isothermal water, an important part of the propagation will be in shallow water under upward-refracting conditions, resulting in small total transmission losses as a result of less bottom interaction. On the other hand, in waters affected by the front, propagation will be under strong downward-refracting conditions, as a result of the steep gradients, and thereby subject to higher losses, particularly at low frequencies. As noted, measurement site B was always in isothermal water, whereas C was periodically subject to the effects of the front. From this, one would expect the transmission losses measured at site B to be both lower in magnitude and subject to less temporal fluctuation than those at site C. Though generally valid, this conclusion is nevertheless based on an oversimplification of the propagation conditions. In particular, the propagation depends not only on the front, but also on frequency, source and receiver depths, bottom conditions (which are different for the two tracks), and, possibly, other features such as currents and inertial oscillations.

3. Selected Results

Figure 2 provides a typical example of the fluctuations in measured transmission loss at site C for several frequencies, along with the predicted tidal curve for the area. It is clear that the fluctuations in transmission loss correlate well with tidal periodicity, particularly for the lower frequencies. This is consistent with the assumption that the lower frequencies are more affected by the tidally induced change in downward-refracting conditions. Both diurnal and semi-diurnal periodicities are evident, the former seemingly the more significant. Further, there is a correspondence, albeit inexact, between high tide and high transmission loss, consistent with the fact that the front reaches site C during periods of high tide. Although the curves shown are for a particular source/receiver combination (240 m/50 m) the observed trends are fairly representative of all the data obtained at this site.

It is instructive to compare the environmental variability at the two positions B and C. An example of the fluctuations in temperature is shown in Fig. 3. It is noted that the corresponding fluctuations in sound speed, not shown here, are very similar, indicating that temperature is the controlling factor in sound speed variations. Several features are immediately evident from the figure. First, it is clear that the amplitudes at C are greater than those at B and, in addition, show a definite dependence on depth. Further, although both data sets reveal tidal effects, they are more conspicuous at position C, particularly at 18-m depth. This behavior no doubt reflects the position of the stations with respect to the Polar front, station C being directly affected by the movements of the front, while station B is constantly in isothermal waters, as discussed earlier. The significant differences in results between the two locations suggest that tidally advected changes in water masses, as at C, are more important than the indirect tidal effects (changes in water depth, currents, etc.) that are evident at B. The greater energy measured at 18 m (for site C) seems to confirm this conclusion, since the transition zone between the Atlantic and Polar waters occurs at this depth. Frequency spectra of the transmission loss, not shown here [5], do lend further support to the above findings.

As a final example of measured results obtained at various source/receiver distances, Fig. 4 [6] shows contours of transmission loss, in 1/3-octave bands, in the frequency/range plane. The plot shows a typical feature of shallow-water (waveguide) propagation--viz., the existence of an "optimum frequency" (here about 250 Hz). The optimum frequency arises from the high attenuation at both high and low frequencies (the former due to absorption and scattering, the latter due to bottom interaction), resulting in an intermediate region of relatively low attenuation.

IV. NUMERICAL MODELING

1. Environmental Model Used

Needless to say, considerable simplification of the actual geoacoustic environment is required for tractable, numerical modeling calculations. As already indicated, the parameters affecting acoustic propagation are dependent both on the spatial and on the temporal variability in the environment. In this case, the water column parameters are both time and range dependent, and the bottom properties are range dependent. For the modeling calculations, the time dependence cannot, of course, be explicitly included. Instead, a few actual sound

speed profiles have been selected to represent the environment at particularly significant times (when the front was either present or absent). For each such condition, the bottom was chosen to be range independent or to vary with range.

2. Typical SAFARI Results

Using SAFARI, numerous runs were made to assess the effects on propagation of varying several of the geoacoustic parameters, particularly the shear rigidity. A flat bottom of 75 m depth was assumed with an isovelocity water column of sound speed 1450 m/s. The other relevant environmental parameters are as follows: a solid bottom with a compressional speed of 1700 m/s, a shear speed of 600 m/s, a compressional attenuation of 0.4 dB/λ, a shear attenuation of 0.8 dB/λ, bottom density 2.0 g/cm^3, and water density 1.0 g/cm^3.

Figure 5 is an example of the behavior of the Green's function integrand for the above choice of parameters and a source frequency of 25 Hz. The source and receiver depths are 70 m and 75 m, respectively; that is, the receiver is on the bottom, and the source is directly above the bottom. The different spectral regions are delineated by their corresponding phase velocities, c_ϕ, and horizontal wavenumbers, k_x, related by $c_\phi = \omega/k_x$, as follows (the critical angle here is 31.5°):

Continuous spectrum: 1700 m/s $< c_\phi$ (propagation angles above 31.5°)
Discrete spectrum: 1450 m/s $\leq c_\phi \leq$ 1700 m/s (angles between horizontal and 31.5°)
Evanscent spectrum: $0 \leq c_\phi <$ 1450 m/s (non-real angles at receiver).

The discrete modes lie in the interval $\omega/c_b < k_x < \text{Max}[\omega/c(z)]$, which in this case is approximately 0.092 to 0.108 m^{-1}, as indicated in the figure. In addition to the dominant discrete mode, there are two continuous modes and an evanescent mode. The evanescent mode is a Scholte interface wave propagating along the bottom with a phase velocity of approximately 525 m/s ($k_x \approx 0.299$ m^{-1}), which is less than that of any of the body waves in this environment (c_w = 1450 m/s, c_b = 1700 m/s, c_s = 600 m/s). Such interface waves (which are sometimes referred to as Stoneley waves) become dominant as the source frequency decreases. At very low frequencies, below the cut-off frequency of discrete mode propagation for bottom-limited (waveguide) environments, these interface waves are often the only effective mechanism for propagation. For the source placed at a depth of 50 m, that is, 25 m above the bottom, it turns out that no interface waves are excited for the preceding conditions. This is not surprising, since the excitation of interface waves diminishes with increasing distance of the source from the bottom, vanishing within a distance of a few shear wavelengths. What this indicates, however, is that interface waves play no role in the experiments reported here.

We now consider a higher frequency. Figure 6 shows the FFP integrand and associated transmission loss for a source frequency of 100 Hz. The source and

receiver were located at a depth of 50 m. The integrand is dominated by a discrete mode of wavenumber approximately equal to 0.43 m^{-1}. In addition, there are two or three smaller amplitude discrete modes, and three or four highly attenuated leaky modes. There are no interface waves in this case. The discrete modes would, therefore, be expected to dominate the farfield propagation. This is clear from the transmission loss curve shown in Figure 6(b). The irregularities in the interference pattern within the first few kilometers are most likely attributable to the leaky modes, which rapidly decay into the bottom at greater ranges. The next 15 km or so display an interference pattern which is almost the typical 2-mode pattern. At greater ranges, the pattern is what one would expect for single-mode propagation.

The significant geoacoustic parameters used in the calculation of the transmission loss for this case are indicated on the figure. It should be noted that the calculation was relatively insensitive to changes in compressional and shear attenuations, β_c and β_s, respectively, resulting in essentially the same transmission loss for several different choices of the parameters. On the other hand, the result was strongly dependent upon the value of shear speed, c_s.

The crosses plotted on the figure represent measured data points taken from Figure 4. Except for a couple of points, the agreement between the measured and calculated results is very good. At long ranges the actual data show greater losses than predicted, possibly reflecting the increasing bottom interaction (and, hence, greater loss) occurring as the energy approaches shallow water. Naturally, the flat bottom assumed by the model cannot account for this effect. In view of the simple environment used in the model, the agreement with measurements is excellent--in fact, misleadingly so. Although the agreement was obtained using only reasonable geoacoustic parameters in the model (i.e., the usual "fiddling" with the model parameters was unnecessary), it does represent a very limited portion of the data set. In particular, only one combination of frequency, source/receiver depths, time, etc., is handled here. It is not obvious that other combinations of these parameters would result in equally good agreement.

3. Typical IFDPE Results

Several runs were made using IFDPE to determine the dependence of TL on source frequency, source and receiver depths and, especially, the position of the Polar Front. One of the environmental models used is shown in Figure 7. The Polar Front is represented by a downward-refracting sound speed profile located approximately 9 km from station A. Two other sound speed profiles are shown, one near station A and the other at station B. Positions in between are filled by the appropriate profile. The vertical lines associated with each profile (at 0, 9, and 52 km) are centered at 1450 m/s, thus serving as a reference for each profile. The bathymetry is indicated by the dashed curve, the steepest slope having a gradient of approximately 1°. The bottom is assumed to be uniformly hard over the track A-B and characterized by a compressional attenuation of 0.8 dB/λ.

FLUCTUATIONS IN ACOUSTIC TRANSMISSION LOSS: COMPARISONS BETWEEN MEASURED DATA AND PREDICTIONS OF THE SAFARI/PARABOLIC EQUATION NUMERICAL MODELS

For several combinations of the relevant parameters and the environmental model in Figure 7, transmission losses were calculated. A typical result is given in Figure 8, which shows an isoloss plot of TL in the range/depth plane for a source frequency of 100 Hz and a source depth of 18 m. Light shading represents high energy concentration (low TL). The first few kilometers are characterized by high energy levels in both the water column and the bottom. The high intensity in the bottom probably corresponds to the radiation of continuous modes into the bottom. Beginning at about 9 km, the start of the front, and terminating beyond 20 km or so, significant coupling of the discrete modes with the bottom appears to be taking place. In particular, we see several beams in the bottom, albeit not well defined, each corresponding to a particular discrete mode. Clearly, the penetration into the bottom of the downward-refracting energy is enhanced by the increasing grazing angle as the energy propagates up slope. Not surprisingly, at the higher frequencies (1 kHz and above) bottom penetration was substantially lower than seen here.

An example of the transmission loss at a particular depth (50 m) for the preceding case is shown in Figure 9. Numerical smoothing has been applied to the curve to remove the large "excursions" typical of PE plots. Although not shown here, the losses indicated in Figure 9 are on the order of 3-5 dB lower than the actual measured values.

The results at other source depths showed surprisingly little difference in TL from the preceding. Moreover, for the 100 Hz case even the removal of the front did not result in as large an effect as was expected and, indeed, measured. The behavior at the higher frequencies, however, in particular at 1500 Hz, was far more sensitive to the front.

CONCLUSIONS

The results described in this paper represent initial attempts to understand a particular data set arising from the propagation of broadband signals in a complex environment. By restricting attention to simple models of a clearly nonsimple situation, we have, at the outset, abandoned hope of being able to explain the detailed behavior, including the temporal fluctuations, of the data. Instead, the objective was to predict the general trends expected and to determine the factors affecting these trends. In this sense, the results are a qualified success. On the one hand, it has been possible to obtain good agreement with the data for some conditions--in fact, much better than expected. On the other hand, the predictions, particularly for the PE model, were relatively insensitive to several obviously important parameters.

REFERENCES

[1] H.B. Ali, 'Spatial and temporal variabilities in underwater acoustic transmission: an analytical review', SACLANTCEN SM-166, La Spezia, Italy, SACLANT ASW Research Centre (1983). [AD 129 959].

[2] H. Schmidt, 'Excitation and propagation of interface waves in a stratified sea-bed,' In: Acoustics and the Sea-Bed, N. G. Pace, ed., Bath Univ. Press, U.K. (1983).

[3] D. Lee and K.E. Gilbert, "Recent Progress in Modeling Bottom Interacting Sound Propagation with Parabolic Equations," In: Oceans 82 Conference Record (MTS-IEEE, Washington, D.C.) pp. 172-177 (1982).

FLUCTUATIONS IN ACOUSTIC TRANSMISSION LOSS: COMPARISONS BETWEEN MEASURED DATA AND PREDICTIONS OF THE SAFARI/PARABOLIC EQUATION NUMERICAL MODELS

[4] J. Pietrzak, and H. B. Ali. Fluctuations in environmental parameters observed during acoustic measurements in the Barents Sea and the Strait of Sicily. La Spezia, Italy, SACLANT ASW Research Centre. (SM-in press).

[5] H. B. Ali, M. C. Ferla, and S. Fiori, 'Medium-Induced Low-Frequency Fluctuations in Acoustic Transmission Loss: Examples from Measurements in Selected Geographical Areas,' In: Ocean Seismo-Acoustics, T. Akal and J. M. Berkson, eds., Plenum Publishing Corporation, N.Y. (1986).

[6] M. C. Ferla, G. Dreini, F. B. Jensen and W. A. Kuperman, 'Broadband model/data comparisons for acoustic propagation in coastal waters,' In: Bottom-Interacting Ocean Acoustics, W. A. Kuperman and F. B. Jensen, eds., Plenum Publishing Corporation, N.Y. (1980).

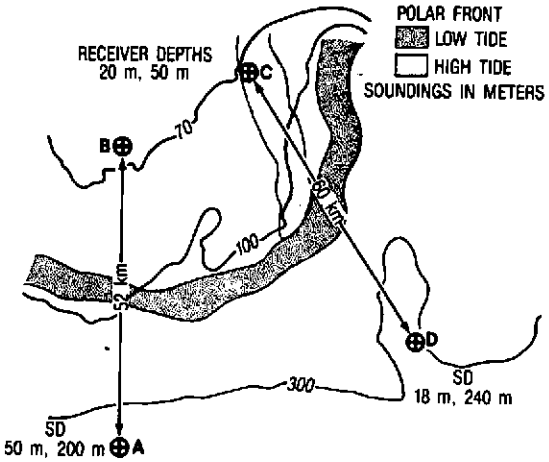

Figure 1 Geometry of the North Atlantic measurements.

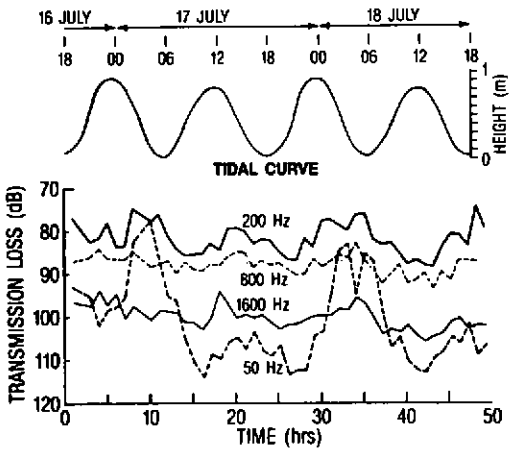

Figure 2. Temporal variation of transmission losses and predicted tidal curve at site C.

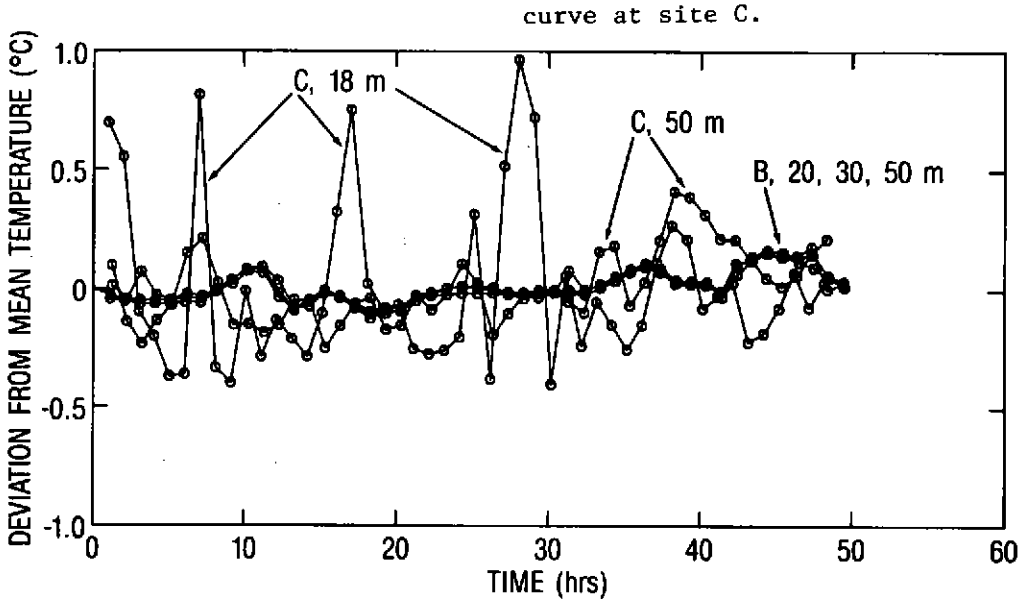

Figure 3. Normalized temperature fluctuations at the two sites.

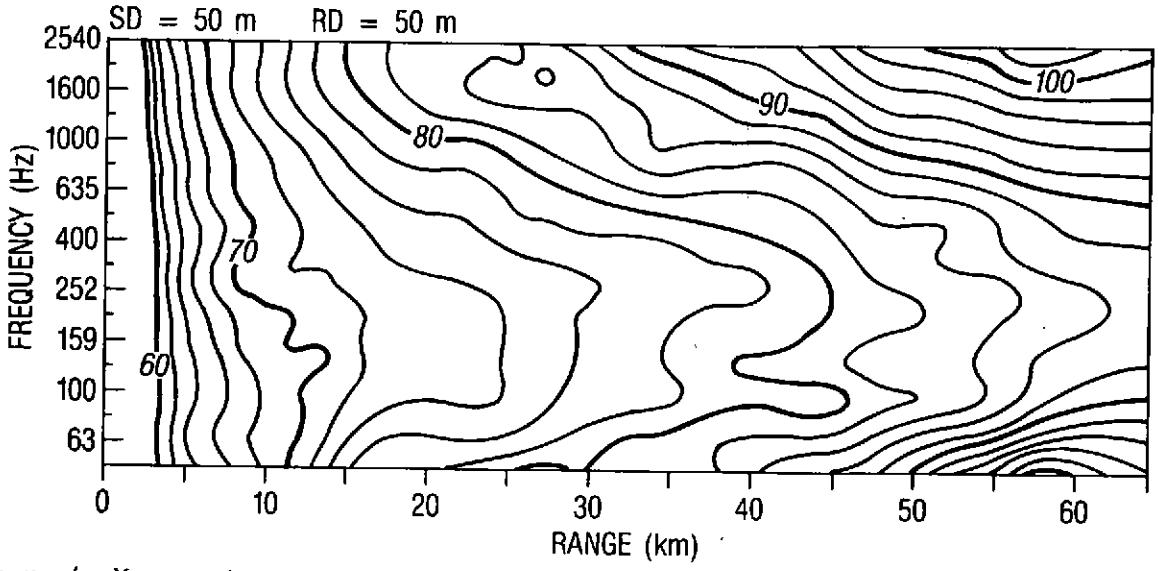

Figure 4. Measured transmission loss contours for up-slope propgation.

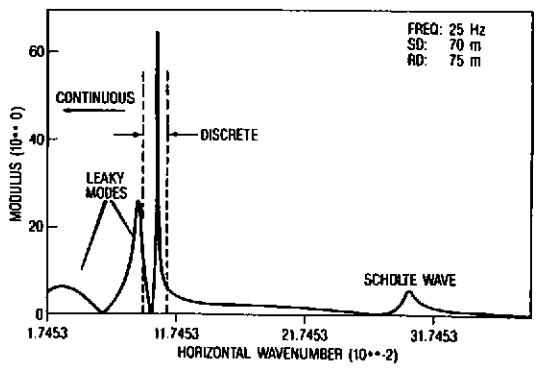

Figure 5. FFP integrand as a function of horizontal wavenumber.

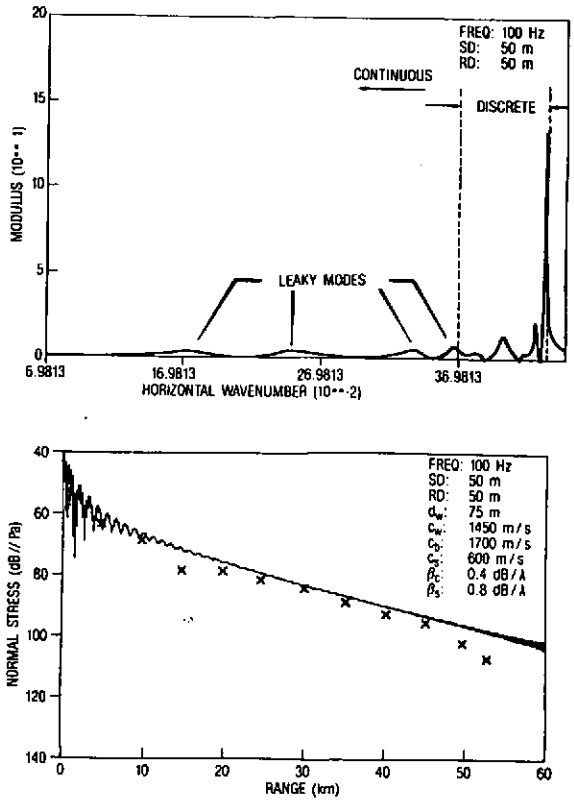

Figure 6. FFP integrand (a) and transmission loss (b).

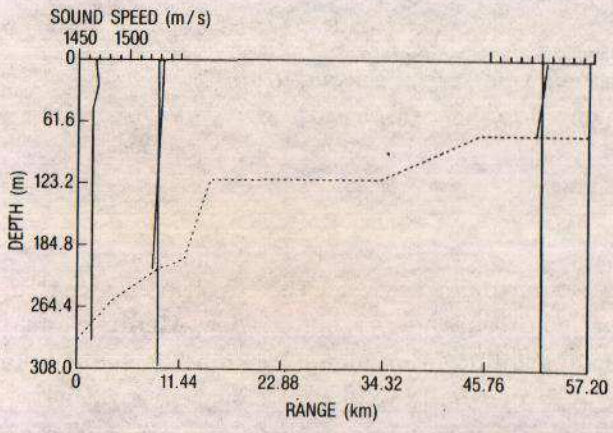

Figure 7. Range-dependent environment for track A-B.

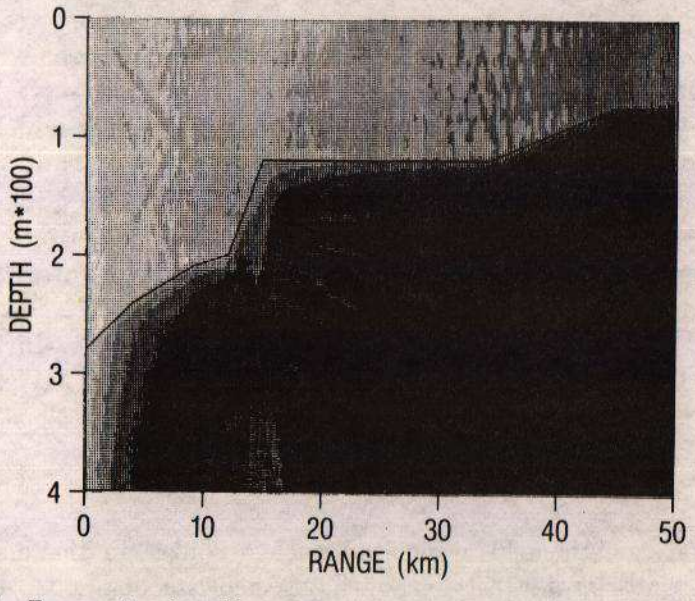

Figure 8. Transmission loss contours along track A-B (source depth 18 m, frequency 100 Hz). (A at range = 0; B at range = 50 km)

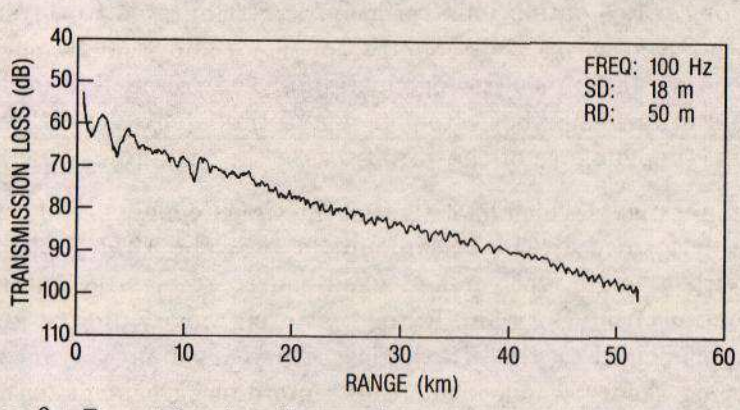

Figure 9. Transmission loss along track A-B at 50 m depth.